JOURNAL OF COMPUTATIONAL PHYSICS **146,** 1–28 (1998)
ARTICLE NO. CP986070

Compatible Fluxes for van Leer Advection

W. B. VanderHeyden and B. A. Kashiwa

Theoretical Division Fluid Dynamics Group, Mail Stop B216, Los Alamos National Laboratory, Los Alamos, New Mexico 87545
E-mail: wbv@lanl.gov, bak@lanl.gov

Received September 25, 1997; revised August 4, 1998

Application of the standard second-order upstream-centered advection method of van Leer to a coupled transport equation system of the form $(\partial/\partial t)[\begin{smallmatrix}\rho\\A\end{smallmatrix}]+\nabla\cdot[\begin{smallmatrix}\rho\\A\end{smallmatrix}]\mathbf{u}=0$ can produce artificial extrema in the ratio $T\equiv A/\rho$, even though T satisfies a simple advection equation and is expected to preserve monotonicity. Here $\mathbf{u}$ is velocity, ρ is mass density, and A is a conserved quantity such as momentum density, energy density, or chemical species density. Thus T is a mass-specific transport quantity such as velocity, energy per unit mass, temperature, or species mass fraction. A new flux formulation and gradient limiting procedure is presented here which eliminates these artificial extrema, preserves the second-order accuracy, and preserves the monotone character of the van Leer method, even in the limit of vanishing mass density. Such a formulation is called *compatible*. The method is noniterative (i.e. explicit) and can be employed in a general finite-volume framework. Sample results for the transport of a square wave in one and two dimensions are provided.

Key Words: finite-difference approximations; synchronous advection; computational fluid dynamics; gradient limiting.

1. INTRODUCTION

This paper introduces a flux formulation that ensures "compatibility" of mass-specific quantities when using an upstream-centered, second-order advection operator. We use compatibility in the sense of Schär and Smolarkiewicz [1], who defined the term in connection with the smoothness of mass-specific quantities such as species mass fraction, velocity, temperature, or specific internal energy. This permits us to reserve the term "monotonicity" for the conserved quantities (species density, momentum density, and energy density). Many second-order advection schemes are monotone, but noncompatible.

0021-9991/98 $25.00

To better understand the meaning of compatibility, consider the system

$$\frac{\partial}{\partial t}\begin{bmatrix}\rho\\ A\end{bmatrix} + \nabla\cdot\begin{bmatrix}\rho\\ A\end{bmatrix}\mathbf{u} = 0, \tag{1.1}$$

where t is time, ρ is the mass density, $\mathbf{u}$ is the velocity, and A is the density of any other conserved quantity such as linear momentum or energy. Such systems arise in numerous applications, including compressible single phase flows, nonisothermal single-phase flows, multispecies flows, and multiphase flows. Note that the above system is also encountered in the numerical solutions of systems with a nonzero right-hand side.

Now, for example, let, $A = \rho T$, and let A be the internal energy density. With unit-specific heat, T is just the temperature. To simplify the discussion we will often refer to A as the energy density, and T as the temperature.

Equation (1.1) implies

$$\rho\frac{dT}{dt} \equiv \rho\left[\frac{\partial T}{\partial t} + \mathbf{u}\cdot\nabla T\right] = 0. \tag{1.2}$$

In other words, the temperature is a Lagrangian invariant. Schär and Smolarkiewicz [1] point out that this means T at a time $t + \Delta t$ must be bounded by the values of T in the immediate neighborhood at time t; they refer to a scheme having this property as being *compatible* with the Lagrangian equations. Such a property is desirable in any numerical advection scheme and can be particularly important in systems having large density gradients, where overshoots and undershoots can be troublesome.

For a typical time-explicit finite-difference or finite-volume method, the solution of the equation system (1.1) is subject to the Courant–Friedrichs–Lewy (CFL) stability criterion based on the transport velocity. This means that information can travel over, at most, one cell per time step. In the terminology of Schär and Smolarkiewicz [1], a *compatible* scheme is one for which the average temperature in a given cell is bounded by the average previous time temperatures from that cell and its neighbors.

Prior efforts to develop compatible advection schemes appear to be limited to the works of Schär and Smolarkiewicz [1] and to Thuburn [2], both of which build upon the idea of flux-corrected transport (FCT). The essence of the FCT idea is to add an anti-diffusive part into an advection scheme based upon upwind differencing, a compatibility constraint being used to gauge the amount of anti-diffusion to be added in. Schär and Smolarkiewicz [1] do so in an iterative fashion within the classical FCT framework. Thuburn [2], in contrast, accomplishes the same goal in a single step. In either case the formula for gauging the allowable amount of anti-diffusion results in so-called "flux-limiting." In contrast to the foregoing prior works, we focus our attention here on a class of upstream-centered methods for advection that make use of *gradient limiting* to ensure monotonicity of the conserved densities. In particular, we shall build upon the multidimensional method introduced by van Leer [3] which is closely related to the scheme of Collela [4] and also to that of Saltzmann [5]. The basic idea behind the method of van Leer [3] is to construct fluxes using a finite Taylor expansion in space about the upstream cell-center, the gradients used in the expansion being "limited" according to a certain recipe involving the neighboring values of the densities. This gradient-limiting procedure can, of course, reduce the scheme locally to a purely upwind (but monotone) method, as is the case for flux-limiting as well.

Hence, our goal is to introduce a flux formulation that renders the multidimensional van Leer advection operator compatible. Achieving this goal will naturally involve a new twist

on gradient limiting. (Our aim is not to introduce an entirely new advection scheme; nor is it to survey the enormous literature on the subject. The reader interested in a broad view of advection schemes should refer to Leveque [6] and the various references cited there.)

It should be noted that we use the term "monotonicity of the advection operator" in the usual colloquial sense. Namely, that for a uniform velocity flow an initially monotonic density distribution will remain monotonic after application of the advection operator. Of course, the van Leer advection scheme that we use in this paper applies to the more general case of nonuniform and divergent velocity fields. In the more general case, velocity divergence acts as a source or sink and can produce new physical density extrema. Since the advection operator can be thought of as a mapping from the Lagrangian (material) frame of reference to the Eulerian (grid) frame [8], it should be expected to map any new physical extrema in density from the Lagrangian data to the mesh without generating spurious new extrema. Fortunately, the conservative form of the advection operator that we employ directly includes the Lagrangian process of compression and expansion. As such, it *automatically* preserves density field monotonicity and any physical extrema generated by divergent flows.

In the next section we examine van Leer's [7] second-order upstream-centered advection scheme, applied to the equation system (1.1), with constant velocity, in one dimension. (As usual we confine our attention to the uniform flow case so that the Lagrangian processes that establish the extrema are not allowed to obscure the mapping process, which is the real interest here.) We show that a standard application of van Leer's scheme is monotone, but noncompatible. The examination reveals the source of the noncompatibility of the standard implementation of van Leer's method. The compatible flux formulation is then developed for the one-dimensional case. Section 3 contains the generalization to multiple space dimensions with general velocity fields, and the corresponding proof of compatibility. In Section 4 we provide example calculations in one and two dimensions to demonstrate the characteristics of the method.

2. THE ONE-DIMENSIONAL CASE

In this section we review the van Leer advection scheme for a one-dimensional advection problem and demonstrate that it is monotone in the conserved quantities for the case of a constant velocity field. We then show that it can lead to noncompatibility. Finally, we show how to alter the flux formulation to render the van Leer scheme compatible.

2.1. *Monotonicity of the van Leer Method*

To begin, we consider the equation system (1.1)

$$\begin{pmatrix} \rho \\ A \end{pmatrix}_t + \begin{pmatrix} \rho u \\ Au \end{pmatrix}_x = 0, \tag{2.1.1}$$

on a one-dimensional domain. We confine our discussion to the case for which $u > 0$ is a constant, a rightward traveling wave. (We will consider the more general case in Section 3.) We use standard finite-difference nomenclature with subscripts denoting the discrete mesh points and superscripts denoting discrete times. Time steps and space increments are denoted by Δt and Δx, respectively. Half-indices denote cell face values. Integrating the equation

system over the jth cell and over time from t^n to $t^n + \Delta t$ we arrive at the standard finite-difference equations for the system

$$q_j^{n+1} = q_j - \sigma \langle q \rangle_{j+1/2} + \sigma \langle q \rangle_{j-1/2}, \tag{2.1.2}$$

where $\sigma = u\Delta t/\Delta x > 0$ is the Courant number and q is either ρ or A. The quantities q_j and q_j^{n+1} are the cell average densities at times t^n and $t^n + \Delta t$, respectively. For convenience, we suppress the superscript n for the time level t^n on the q's.

The angle bracket quantities denote the fluxed quantities given by

$$\langle q \rangle_{j+1/2} = \frac{1}{\Delta t} \int_{t^n}^{t^n+\Delta t} q(x_{j+1/2}, t)\, dt, \tag{2.1.3}$$

where q is either ρ or A. As is commonly known, first-order accuracy is obtained by assuming the quantity $q(x_{j+1/2}, t)$ is a constant and is given by the cell average value upstream from the face, i.e. $q(x_{j+1/2}, t) \approx q_j$.

Higher accuracy is obtained by recognizing that $q(x_{j+1/2}, t)$ is not, in general, a constant over the time interval t^n to $t^n + \Delta t$. A second-order accurate method results from approximating the distribution of q at time t^n in each cell as a linear function of space, that is

$$q(x, t^n) \approx q_j + \left(\frac{\partial q}{\partial x}\right)_j (x - x_j), \tag{2.1.4}$$

which provides a piecewise-linear representation of $q(x, t^n)$ over the domain. Using Eq. (2.1.4) with the transformation, $q(x_{j+1/2}, t) = q[x_{j+1/2} - u(t - t^n), t^n]$ in Eq. (2.1.3) gives a space-time centered approximation for the fluxed quantities,

$$\langle q \rangle_{j+1/2} = q_j + \left(\frac{\partial q}{\partial x}\right)_j \frac{\Delta x_j}{2}(1 - \sigma), \tag{2.1.5}$$

where $\Delta x_j = x_{j+1/2} - x_{j-1/2}$. It is well known that nonmonotone solutions to the equation system (2.1.1) can result from the from the use of straightforward numerical approximations to the spatial derivative in Eq. (2.1.5). The origin of the problem is nonmonotonicity of the piecewise-linear representation of q by the set of Eqs. (2.1.4). Van Leer [6] resolved this problem by *limiting* the numerical spatial derivatives so that the piecewise-linear density fields preserve monotonicity, while producing the highest possible accuracy. (We loosely refer to van Leer's method as second-order accurate, which is only true in areas where the solution varies smoothly.) Let $\bar{\Delta}_j$ denote van Leer's *limited* difference operator. Van Leer's prescription is

$$\bar{\Delta}_j q = \begin{cases} \min[4|q_j - q_{j-1}|, |q_{j+1} - q_{j-1}|, 4|q_{j+1} - q_j|]\,\mathrm{sign}[q_{j+1} - q_{j-1}], \\ \qquad \text{if } \mathrm{sign}[q_j - q_{j-1}] = \mathrm{sign}[q_{j+1} - q_{j-1}] = \mathrm{sign}[q_{j+1} - q_j], \\ 0, \qquad \text{otherwise.} \end{cases} \tag{2.1.6}$$

The spatial derivative in Eqs. (2.1.4)–(2.1.5) is then approximated as

$$\left(\frac{\partial q}{\partial x}\right)_j \approx \frac{\bar{\Delta}_j q}{2\Delta x_j}. \tag{2.1.7}$$

In doing so, we are assured that the cell face values (the extrema for each cell) given by

$$q_{j+1/2^{(L)}} = q_j + \frac{1}{4}\bar{\Delta}_j q \tag{2.1.8a}$$

and

$$q_{j-1/2^{(R)}} = q_j - \frac{1}{4}\bar{\Delta}_j q, \tag{2.1.8b}$$

where the superscripts (L) and (R) denote the values approaching from the left and right, respectively, are bounded by the neighboring cell-center data (e.g., $q_j \le q_{j+1/2^{(L)}} \le q_{j+1}$).

Using Eqs. (2.1.5), (2.1.7), (2.1.8a), (2.1.8b), we obtain expressions for the fluxes in terms of the bounded face values of q:

$$\langle q \rangle_{j+1/2} = \sigma q_j + (1-\sigma) q_{j+1/2^{(L)}} \tag{2.1.9a}$$

and

$$\langle q \rangle_{j-1/2} = \sigma q_{j-1} + (1-\sigma) q_{j-1/2^{(L)}}. \tag{2.1.9b}$$

From Eqs. (2.1.9a)–(2.1.9b) we can see that the fluxes are weighted averages of the face- and cell-centered data for $0 \le \sigma \le 1$ and are, therefore, also bounded by the surrounding cell-centered data for this Courant number range.

Now we are ready to verify the monotonicity of van Leer's advection scheme. Using Eq. (2.1.9a) we can express the quantity $q_j - \sigma \langle q \rangle_{j+1/2}$ as

$$q_j - \sigma \langle q \rangle_{j+1/2} = (1-\sigma) q_{re}, \tag{2.1.10}$$

where

$$q_{re} \equiv (1-\sigma) q_j + \sigma q_{j-1/2^{(R)}}. \tag{2.1.11}$$

The quantity $(1-\sigma)q_{re}$ can be thought of as the density of material *remaining* in the cell after the outgoing flux is withdrawn if the inflow flux were neglected. (Notice the linear gradients ensure $q_{j+1/2^{(L)}} - q_j = q_j - q_{j-1/2^{(R)}}$, which is used to obtain Eq. (2.1.10).)

Now for $0 \le \sigma \le 1$, q_{re} is a weighted average of the cell-center and face data and is therefore, itself, bounded by the surrounding cell-center data. From Eqs. (2.1.2) and (2.1.10) we obtain, finally,

$$q_j^{n+1} = (1-\sigma) q_{re} + \sigma \langle q \rangle_{j-1/2}. \tag{2.1.12}$$

Thus, q_j^{n+1} is a weighted average of two bounded quantities, q_{re} and $\langle q \rangle_{j-1/2}$, with interpolant σ. Hence, van Leer's scheme is monotone if the interpolant satisfies $0 \le \sigma \le 1$, which, of course, is well known [7].

It is also well known that the first-order limit of Eq. (2.1.12),

$$q_j^{n+1} = (1-\sigma) q_j + \sigma q_{j-1}, \tag{2.1.13}$$

is also monotone for the same conditions on σ. What is not so obvious is the source of noncompatibility of Eq. (2.1.12), which is studied next.

2.2. *Noncompatibility of the Standard van Leer Method*

We now examine the compatibility of the foregoing method applied to the system (1.1). In particular we shall study the smoothness of the mass-specific quantity $T = A/\rho$ (temperature). Using Eq. (2.1.12) for the densities ρ and A, we obtain, after some manipulation,

$$T_j^{n+1} = (1 - Q)\frac{A_{re}}{\rho_{re}} + Q\frac{\langle A\rangle_{j-1/2}}{\langle\rho\rangle_{j-1/2}}, \tag{2.2.1a}$$

where

$$Q = \frac{\sigma\langle\rho\rangle_{j-1/2}}{(1-\sigma)\rho_{re} + \sigma\langle\rho\rangle_{j-1/2}}. \tag{2.2.1b}$$

If van Leer's limited differences are used to form the second-order mass density fluxes, we are assured that $0 \le Q \le 1$ for $0 \le \sigma \le 1$.[1] In this range, we see that the new temperature is a weighted average of the ratios A_{re}/ρ_{re} and $\langle A\rangle_{j-1/2}/\langle\rho\rangle_{j-1/2}$. These ratios can also be considered temperatures. The former is the temperature of the material "remaining" in the cell considering outflows only, while the latter is the temperature of the material entering the cell. We have compatibility if these ratios are bounded by the surrounding temperature data. Unfortunately, because spatial distributions of ρ and A are independent (that is, no information regarding the cell-center temperatures is directly included in limiting the fluxes of A) these ratios are not generally bounded by the surrounding temperature data; hence, the scheme is not generally compatible.

In contrast, for the first-order case, Eqs. (2.2.1a)–(2.2.1b) reduce to

$$T_j^{n+1} = (1 - Q)T_j + QT_{j-1}, \tag{2.2.2a}$$

where now

$$Q = \frac{\sigma\rho_{j-1}}{(1-\sigma)\rho_j + \sigma\rho_{j-1}}. \tag{2.2.2b}$$

This simplification occurs because the energy fluxes, $\langle A\rangle$, in the first-order case are simply products of cell-center mass densities and temperatures. As a result, the mass density factors out of the the ratios encountered in Eq. (2.2.1a).

Thus, for the first-order case, T_j^{n+1} is bounded by T_j and T_{j-1} for $0 \le \sigma \le 1$, even in the limit of vanishing mass. In this case $\sigma > 0$ and ρ_{j-1} vanishes before ρ_j, so that $Q \to 0$ and $T_j^{n+1} \to T_j$.

Whereas the first-order scheme lacks the desired accuracy, it yields both monotone densities and compatible temperatures and is well-behaved in the limit of vanishing mass. The second-order compatible fluxes developed in the next section will be shown to recover these properties and to retain second-order accuracy.

2.3. *Compatible Fluxes for van Leer's Operator*

The compatibility of the first-order upwind scheme, demonstrated in the previous section, is related to the fact that the fluxed energies, $\langle A\rangle$, are products of cell-center mass densities

[1] For the case $\rho_{re} = \langle\rho\rangle_{j-1/2} = 0$, Q is, strictly speaking, undefined. In a practical calculation, however, one may add a small amount of residual density to the denominator in Eq. (2.2.1b) to force $Q \to 0$ in this limit.

and temperatures. For example, $\langle A\rangle_{j-1/2} = \rho_{j-1}T_{j-1}$. This characteristic ensured that the "remaining" and fluxed temperatures, A_{re}/ρ_{re} and $\langle A\rangle_{j-1/2}/\langle\rho\rangle_{j-1/2}$, respectively, were bounded by the surrounding cell-center data.

In what follows, we introduce a new second-order definition of the fluxed energy density that renders van Leer's method compatible. We start with the Taylor expansion of the field $A = \rho T$ in each cell and expand the first-order spatial derivative using the product rule. Thus, for the jth cell

$$A = \rho T = T_j\left[\rho_j + \left(\frac{\partial\rho}{\partial x}\right)_j (x - x_j)\right] + \rho_j\left(\frac{\partial T}{\partial x}\right)_j (x - x_j) + \mathcal{O}\big[(x - x_j)^2\big]. \quad (2.3.1)$$

The Taylor expansion for mass density is

$$\rho = \rho_j + \left(\frac{\partial\rho}{\partial x}\right)_j (x - x_j) + \mathcal{O}\big[(x - x_j)^2\big].$$

If we neglect the terms of $\mathcal{O}[(x-x_j)^2]$ in the above expansions and form the ratio $T = A/\rho$, we obtain the following piecewise nonlinear spatial temperature distribution in the presence of density gradients:

$$T = T_j + \frac{\rho_j(\partial T/\partial x)_j(x - x_j)}{\rho_j + (\partial\rho/\partial x)_j(x - x_j)}. \quad (2.3.2)$$

This nonlinear distribution is crucial; it will enable us to construct a limited difference operator for temperature that produces compatible fluxes. From Eq. (2.3.2) we see that the relation

$$T_{\min} - T_j \le \frac{\rho_j\left(\frac{\partial T}{\partial x}\right)_j (x - x_j)}{\rho_j + \left(\frac{\partial\rho}{\partial x}\right)_j (x - x_j)} \le T_{\max} - T_j, \quad (2.3.3)$$

must hold if compatibility of the temperature field is to be obtained, where $T_{\min}$ and $T_{\max}$ are the minimum and maximum of the local cell-center temperatures. To enforce inequality (2.3.3), we introduce a new limited temperature difference operator. Due to the nonlinearity of the temperature field, this operator is different from the limited difference operator for the density fields given by Eq. (2.1.6). Let $\tilde{\Delta}$ denote the new operator for the temperature. For the one-dimensional case we introduce the prescription

$$\rho_j\tilde{\Delta}_j T = \min\begin{bmatrix} 4|T_j - T_{j-1}|\big(\rho_j - \frac{1}{4}\bar{\Delta}_j\rho\big), \\ |T_{j+1} - T_{j-1}|\rho_j, \\ 4|T_{j+1} - T_j|\big(\rho_j + \frac{1}{4}\bar{\Delta}_j\rho\big) \end{bmatrix}\operatorname{sign}[T_{j+1} - T_{j-1}] \quad (2.3.4a)$$

if $\operatorname{sign}[T_j - T_{j-1}] = \operatorname{sign}[T_{j+1} - T_{j-1}] = \operatorname{sign}[T_{j+1} - T_j]$, and

$$\rho_j\tilde{\Delta}_j T = 0 \quad (2.3.4b)$$

otherwise. Hence, the operator $\tilde{\Delta}_j T$ is simply van Leer's operator, Eq. (2.1.6), applied to a field having a nonlinear distribution like (2.3.2). Notice that if the mass density approaches zero (on average or on a cell face), the limited temperature difference is forced to zero, the

first-order limit, by this prescription. This is a key feature of the new formulation. To be consistent with the monotone mass density representation and to include the proper density variation characteristics, the limited mass density difference, $\bar{\Delta}_j \rho$, is used in Eq. (2.3.4a). Setting $\rho_j (\partial T/\partial x)_j = \rho_j \tilde{\Delta}_j T/2\Delta x_j$, the limited temperature field in each cell is now

$$T = T_j + \frac{\rho_j \tilde{\Delta}_j T \left(\frac{x-x_j}{2\Delta x_j}\right)}{\rho_j + \bar{\Delta}_j \rho \left(\frac{x-x_j}{2\Delta x_j}\right)}. \tag{2.3.5}$$

Equation (2.3.5) guarantees face temperatures that are bounded by the surrounding cell-center temperature data. That is, for example, $T_j \le T_{j+1/2^{(L)}} \le T_{j+1}$. (The reader can quickly verify that the extrema in Eq. (2.3.5) are at the cell faces.)

We can now examine the implications of the expansion (2.3.1) using the new limited temperature difference on the fluxed energies. From Eqs. (2.1.5) and (2.3.1) and setting $\rho_j (\partial T/\partial x)_j = \rho_j \tilde{\Delta}_j T/2\Delta x_j$, we find the fluxed energies to be

$$\langle A \rangle_{j-1/2} = \sigma \rho_{j-1} T_{j-1} + (1-\sigma) \rho_{j-1/2^{(L)}} T_{j-1/2^{(L)}} \tag{2.3.6a}$$

and

$$\langle A \rangle_{j+1/2} = \sigma \rho_j T_j + (1-\sigma) \rho_{j+1/2^{(L)}} T_{j+1/2^{(L)}}. \tag{2.3.6b}$$

For $0 \le \sigma \le 1$ the fluxed energies are weighted averages of the cell-centered energy density, and the face energy density. The reader can verify that the limited differences ensure that the flux of A given by Eq. (2.3.6b) is bounded by the surrounding data and therefore preserves the monotonicity of the van Leer scheme.

Compatibility of the temperature for the new formulation is demonstrated by using Eqs. (2.3.6a)–(2.3.6b), and (2.2.1a) to obtain

$$T_j^{n+1} = (1-Q)\hat{T}_{re} + Q\hat{T}_{in}, \tag{2.3.7}$$

where Q is given by Eq. (2.2.1b), and

$$\hat{T}_{re} = \left[\frac{\rho_j T_j - \sigma \langle \rho T \rangle_{j+1/2}}{\rho_j - \sigma \langle \rho \rangle_{j+1/2}}\right] \tag{2.3.8}$$

and

$$\hat{T}_{in} = \frac{\langle \rho T \rangle_{j-1/2}}{\langle \rho \rangle_{j-1/2}}. \tag{2.3.9}$$

The scheme will be compatible as long as $0 \le Q \le 1$ and both $\hat{T}_{re}$ and $\hat{T}_{in}$ are bounded by the surrounding cell-center data. We have already argued that $0 \le Q \le 1$ for $0 \le \sigma \le 1$. So the remaining task is to find the conditions under which $\hat{T}_{re}$ and $\hat{T}_{in}$ are bounded by surrounding cell-center temperature data. Let us first examine $\hat{T}_{in}$, which is simply the average temperature of the inflow material. From Eqs. (2.1.9b) and (2.3.6a)

$$\begin{aligned} \hat{T}_{in} &= \frac{\sigma (\rho T)_{j-1} + (1-\sigma)(\rho T)_{j-1/2^{(L)}}}{\sigma \rho_{j-1} + (1-\sigma)\rho_{j-1/2^{(L)}}} \\ &= \omega_{in} T_{j-1} + (1-\omega_{in}) T_{j-1/2^{(L)}}, \end{aligned} \tag{2.3.10a}$$

where

$$\omega_{in} = \frac{\sigma\rho_{j-1}}{\sigma\rho_{j-1} + (1-\sigma)\rho_{j-1/2^{(L)}}}. \tag{2.3.10b}$$

For the interval $0 \le \sigma \le 1$ with nonzero mass densities we have $0 \le \omega_{in} \le 1$. Furthermore, for the vanishing mass case in a rightward traveling wave, we expect ω_{in} to tend to zero, since ρ_{j-1} will approach zero faster than $\rho_{j-1/2^{(L)}}$. Thus, T_{in} is a weighted average of T_{j-1} and $T_{j-1/2^{(L)}}$. Because $T_{j-1/2^{(L)}}$ is bounded by T_{j-1} and T_j, so then is $\hat{T}_{in}$.

Now consider $\hat{T}_{re}$. This quantity can be thought of as the temperature "remaining" if only outflow is considered. Using Eqs. (2.1.9a), (2.3.6b), and (2.3.8) we see that

$$\begin{aligned} \hat{T}_{re} &= \frac{(\rho T)_j - \sigma[\sigma(\rho T)_j + (1-\sigma)(\rho T)_{j+1/2^{(L)}}]}{\rho_j - \sigma[\sigma\rho_j + (1-\sigma)\rho_{j+1/2^{(L)}}]} \\ &= (1-\omega_{re})T_j + \omega_{re}T_{j-1/2^{(R)}}, \end{aligned} \tag{2.3.11a}$$

where

$$\omega_{re} = \frac{\sigma\rho_{j-1/2^{(R)}}}{(1-\sigma)\rho_j + \sigma\rho_{j-1/2^{(R)}}}. \tag{2.3.11b}$$

For the interval $0 \le \sigma \le 1$ with nonzero mass densities we have $0 \le \omega_{re} \le 1$. For the vanishing mass case in a rightward traveling wave, we expect $\omega_{re} \to 0$ since $\rho_{j-1/2^{(R)}}$ will approach zero faster than ρ_j. So, in this limit, $\hat{T}_{re} \to T_j$. Thus, $\hat{T}_{re}$ is a weighted average of T_j and $T_{j-1/2^{(R)}}$. Since $T_{j-1/2^{(R)}}$ is bounded by T_{j-1} and T_j, so is $\hat{T}_{re}$. Finally then, T_j^{n+1} is bounded by the surrounding cell-center temperatures; compatibility is proved and the new fluxes produce a van Leer scheme with the desirable vanishing-mass properties seen for the first-order case.

To recap this one-dimensional development, we have shown how the flux of a conserved quantity, $A = \rho T$, can be developed so as to render van Leer's advection operator both monotone in the conserved quantity and compatible in the mass-specific quantity, T. The first step is to use the product rule for differentiation of ρT so that the fluxed ρT can be expressed as a linear combination of products of mass density and temperatures at the cell centers and cell faces as in Eqs. (2.3.6a)–(2.3.6b). The second step is to recognize the nonlinearity of the temperature that results from assuming a linear distribution in ρT and to introduce an appropriate nonlinear limited difference operator so face values are bounded by the surrounding temperature data. Use of the limited nonlinear T differences will guarantee monotonicity of ρT and compatibility of T in a second-order scheme without changing the conditions on the Courant number for stability or monotonicity.

The gradient-limited advection algorithm using the new compatible flux formulation is then:

- Compute trial gradients for densities and temperatures.
- Limit mass density gradients using the standard linear form.
- Limit temperature or mixing ratio gradients according to the nonlinear form.
- Compute the fluxed quantities with limited gradients.
- Perform the straightforward advection operation.

3. GENERAL MULTIDIMENSIONAL COMPATIBLE SCHEME

The compatible flux formulation developed in the previous section for the one-dimensional case can be extended to the multidimensional, arbitrary-velocity-field case in a relatively

straightforward and similar manner. We outline the steps in this section for an unsplit (with regard to mesh direction) time-explicit multidimensional arbitrary finite-volume van Leer advection scheme. Note that the advection operator used in the following development is equivalent to that developed by van Leer [3] for multidimensional advection. The monotonicity characteristics will be preserved. The new contribution will be the formulation of compatible fluxes.

3.1. *Finite Control Volume Conservation Equations*

The fundamental control volume description for the conservation equation system (1.1) is

$$\frac{d}{dt}\int_{V(t)} q\,dV + \int_{S(t)} q(\mathbf{u}-\mathbf{u}_s)\cdot\mathbf{n}\,dS = 0, \tag{3.1.1}$$

where q is either ρ or A. $V(t)$ is an arbitrary time-varying control volume, $S(t)$ is its surface, $\mathbf{u}_s$ is the surface velocity, and $\mathbf{n}$ is the outward unit vector normal to the surface [10]. To simplify the discussion, let us consider here the case of a stationary mesh for which $\mathbf{u}_s = 0$.

We wish to solve these equations on an arbitrary finite-volume mesh. We start by applying Eq. (3.1.1) to the jth control volume or cell of the mesh and approximate the time derivative with a first-order forward-difference formula. Let q_j denote a cell volume average

$$q_j = \frac{1}{V_j}\int_{V_j} q(\mathbf{x}, t^n)\,dV, \tag{3.1.2}$$

where $\mathbf{x}$ is the position vector and V_j is the volume of the jth cell. The conservation equations take the form

$$q_j^{n+1}V_j = q_jV_j - \Delta t\int_{S_j} q\mathbf{u}\cdot\mathbf{n}\,dS, \tag{3.1.3}$$

where S_j denotes the jth cell surface. If one breaks up the surface integral in Eq. (3.1.3) into segments corresponding to inflowing and outflowing volumes, one finds, after making use of the Gauss theorem and some manipulation that

$$q_j^{n+1}V_j = q_jV_j - \sum_o \langle q\rangle_o \Delta V_o + \sum_i \langle q\rangle_i \Delta V_i, \tag{3.1.4}$$

where the subscripts o and i denote sections of the jth cell surface undergoing outflow and inflow, respectively. Each outflow and inflow section will have an associated fluxed volume denoted by ΔV_o and ΔV_i, respectively. This fluxed volume is the volume of material which passes through each surface section in the time increment Δt. The angle brackets denote the average of the quantity over the fluxed volume at time t^n:

$$\langle q\rangle = \frac{1}{\Delta V}\int_{\Delta V} q(\mathbf{x}, t^n)\,dV. \tag{3.1.5}$$

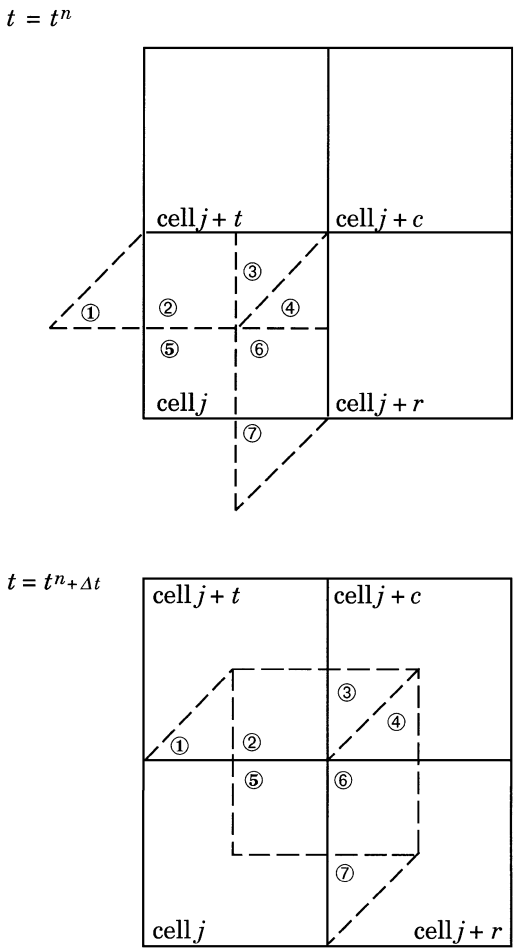

FIG. 1. Fluxed volumes.

To clarify the terms so far take, for example, the case of a Cartesian mesh with $\Delta x = \Delta y = 1$ and with x, y velocity components $u = v = 1$. Suppose, further, $\Delta t = 0.5$. The fluxed volumes associated with upper and right faces of cell j at time t^n and t^{n+1} are shown in Fig. 1.

The figure shows each volume that passes through the right and upper faces of cell j. In the example, volumes 2, 3, 4, and 6 are outflow volumes for cell j. Volumes 1 and 2 are inflow volumes for cell $j + t$. Volumes 3 and 4 are inflow volumes for cell $j + c$. Volumes 6 and 7 are inflow volumes for cell $j + r$. The volume labeled 5 remains in cell j. The reader may consult Collela [3] for more discussion on the geometric description of the fluxed volumes in multidimensional advection calculations.

3.2. *Inflow and Outflow Effects*

We can now manipulate Eq. (3.1.4) to show how to treat the fluxed quantities to ensure compatibility of the multidimensional van Leer advection scheme. Our aim is to show that the new temperature is a weighted average of the value for the jth cell and its neighbors.

We start by setting $q = \rho T$ in Eq. (3.1.4) and simply grouping the terms as

$$(\rho T)_j^{n+1} V_j = \left\{ (\rho T)_j V_j - \sum_o \langle \rho T \rangle_o \Delta V_o \right\} + \sum_i \langle \rho T \rangle_i \Delta V_i. \tag{3.2.1}$$

The curly brace term will be recognized as the energy remaining in the cell considering outflow only; the last term is the inflowing energy. If we multiply and divide the terms in the inflow sum by the inflowing fluxed densities we obtain

$$(\rho T)_j^{n+1} V_j = \left\{ (\rho T)_j V_j - \sum_o \langle \rho T \rangle_o \Delta V_o \right\} + \sum_i \langle \rho \rangle_i \frac{\langle \rho T \rangle_i}{\langle \rho \rangle_i} \Delta V_i. \tag{3.2.2}$$

Now multiply and divide the inflow sum by the total inflowing mass to get

$$\begin{aligned}(\rho T)_j^{n+1} V_j = & \left\{ (\rho T)_j V_j - \sum_o \langle \rho T \rangle_o \Delta V_o \right\} \\ & + \left\{ \sum_i \langle \rho \rangle_i \Delta V_i \right\} \sum_i \frac{\langle \rho \rangle_i}{\left\{ \sum_i \langle \rho \rangle_i \Delta V_i \right\}} \frac{\langle \rho T \rangle_i}{\langle \rho \rangle_i} \Delta V_i. \end{aligned} \tag{3.2.3}$$

Let us now define, as in the one-dimensional case, an auxiliary quantity $\hat{T}_{re}$ as

$$\hat{T}_{re} \equiv \frac{(\rho T)_j V_j - \sum_o \langle \rho T \rangle_o \Delta V_o}{\rho_j V_j - \sum_o \langle \rho \rangle_o \Delta V_o}. \tag{3.2.4}$$

This is the net temperature of the material in the cell that is not fluxed out, neglecting inflow. Let us also define $\hat{T}_{in}$ as

$$\hat{T}_{in} \equiv \sum_i \frac{\langle \rho \rangle_i}{\left\{ \sum_i \langle \rho \rangle_i \Delta V_i \right\}} \frac{\langle \rho T \rangle_i}{\langle \rho \rangle_i} \Delta V_i. \tag{3.2.5}$$

This is the net average temperature of all materials fluxed into the cell. With these definitions, Eq. (3.2.3) takes the form:

$$(\rho T)_j^{n+1} V_j = \left\{ \rho_j V_j - \sum_o \langle \rho \rangle_o \Delta V_o \right\} \hat{T}_{re} + \left\{ \sum_i \langle \rho \rangle_i \Delta V_i \right\} \hat{T}_{in}. \tag{3.2.6}$$

Dividing through by the new mass, $\rho_j^{n+1} V_j$, and using Eq. (3.1.4) we obtain

$$T_j^{n+1} = (1 - Q) \hat{T}_{re} + Q \hat{T}_{in}, \tag{3.2.7}$$

where Q is given by

$$Q = \frac{m_{in}}{m_{re} + m_{in}},$$

with

$$m_{in} = \sum_i \langle \rho \rangle_i \Delta V_i$$

and

$$m_{re} = \rho_j V_j - \sum_o \langle \rho \rangle_o \Delta V_o.$$

From Eqs. (3.2.7) we can see that the new temperature is a weighted average of the quantities $\hat{T}_{in}$ and $\hat{T}_{re}$, provided $0 \le Q \le 1$. We now must show, as in the one-dimensional case, the conditions under which $0 \le Q \le 1$, and both $\hat{T}_{in}$ and $\hat{T}_{re}$ are bounded by the surrounding cell-center temperatures.

Let us first examine the bounds on Q. We start with a limited piecewise-linear representation for ρ. Within each cell,

$$\rho = \rho_j + (\nabla \rho)_j \cdot \mathbf{r}_j, \tag{3.2.8}$$

where $\mathbf{r}_j = \mathbf{x} - \mathbf{x}_j$ is the position vector relative to the cell volume centroid, $\mathbf{x}_j$. We may use Eq. (3.2.8) in Eq. (3.1.5) to compute the mass average densities in an arbitrary volume, ΔV, in the jth cell as

$$\langle \rho \rangle = \rho_j + (\nabla \rho)_j \cdot \langle \mathbf{r}_j \rangle. \tag{3.2.9}$$

The quantity $\langle \mathbf{r}_j \rangle$ is the volume centroid of ΔV.

In what follows, we assume that the gradients in Eqs. (3.2.8)–(3.2.9) are limited so that the extrema in each segment of the piecewise-linear representation of the density are bounded by the surrounding mesh data. Dukowicz and Kodis [8] provide a multidimensional version of van Leer's limiter for an arbitrary quantity q. In their method, a trial gradient is computed by standard means and then limited by multiplication by a coefficient, α_j:

$$(\nabla q)_j \to \alpha_j (\nabla q)_j. \tag{3.2.10a}$$

The coefficient α_j is computed by ensuring the vertex values of q computed from the Taylor expansion involving $\alpha_j\ (\nabla q)_j$ do not lie outside the maximum, $q_{\max}$, and minimum, $q_{\min}$, of the surrounding cell-center data. This yields the prescription for α_j,

$$\alpha_j = \min[1, \alpha_{\max}, \alpha_{\min}], \tag{3.2.10b}$$

where

$$\alpha_{\max} = \max\left[0, \frac{q_{\max} - q_j}{\max[q_v] - q_j}\right] \tag{3.2.10c}$$

and

$$\alpha_{\min} = \max\left[0, \frac{q_{\min} - q_j}{\min[q_v] - q_j}\right], \tag{3.2.10d}$$

where q_v are the values of q at the cell vertices computed using the linear expansion for q, such as Eq. (3.2.8), with the trial density gradient. Since the vertex values are the extrema for the linear expansion, this procedure guarantees that the densities are bounded by the surrounding cell-center data. (It is important to point out here that other gradient-limiting procedures may be used as well. The following discussion only requires that the extrema of each segment of the piecewise function remain bounded by the surrounding mesh data.)

If the mass density gradient used in Eqs. (3.2.8)–(3.2.9) is limited we are assured that the mass fluxes and therefore m_{in} are nonnegative, since the centroids of the fluxed volumes are all within their respective cells. Then, as in the one-dimensional case, if $m_{re} > 0$, we have $0 \le Q \le 1$. Let us now examine m_{re}.

If we use Eq. (3.2.9) in the formula for m_{re} we obtain

$$m_{re} = \rho_j \left[V_j - \sum_o \Delta V_o \right] - (\nabla \rho)_j \cdot \sum_o \langle \mathbf{r}_j \rangle_o \Delta V_o. \tag{3.2.11}$$

Let us define an auxiliary position vector, $\mathbf{r}_j^\star$ as

$$\mathbf{r}_j^\star \equiv \frac{-\sum_o \langle \mathbf{r}_j \rangle_o \Delta V_o}{\left[V_j - \sum_o \Delta V_o \right]}. \tag{3.2.12}$$

If one chooses a numerical advection scheme so that none of the fluxed volumes, ΔV_o, overlap, then it is easy to show that $\mathbf{r}_j^\star$ is the centroid of the volume in the cell that is not fluxed out—i.e. the "remaining" material. In Fig. 1, for example, this would be the centroid of volume 5. To show this, recognize that since $\mathbf{r}_j$ is defined relative to the cell centroid we have the relationship

$$\begin{aligned} \int_{V_j} \mathbf{r}_j \, dV &= 0 \\ &= \sum_o \int_{\Delta V_o} \mathbf{r}_j \, dV + \int_{V_j - \sum_o \Delta V_o} \mathbf{r}_j \, dV \\ &= \sum_o \langle \mathbf{r}_j \rangle_o \Delta V_o + \left[V_j - \sum_o \Delta V_o \right] \langle \mathbf{r}_j \rangle_{re}, \end{aligned} \tag{3.2.13}$$

where the centroid of the "remaining" material is defined as

$$\langle \mathbf{r}_j \rangle_{re} \equiv \frac{1}{V_j - \sum_o \Delta V_o} \int_{V_j - \sum_o \Delta V_o} \mathbf{r}_j \, dV. \tag{3.2.14}$$

From Eqs. (3.2.13)–(3.2.14) it is clear that, provided the volumes ΔV_o do not overlap,

$$\langle \mathbf{r}_j \rangle_{re} = \mathbf{r}_j^\star = \frac{-\sum_o \langle \mathbf{r}_j \rangle_o \Delta V_o}{\left[V_j - \sum_o \Delta V_o \right]}. \tag{3.2.15}$$

Now, if we use definition (3.2.12) in Eq. (3.2.11) we obtain

$$m_{re} = \left[V_j - \sum_o \Delta V_o \right] [\rho_j + (\nabla \rho)_j \cdot \mathbf{r}_j^\star]. \tag{3.2.16}$$

So m_{re} is made up of two factors, both of which must be nonnegative for m_{re} to be nonnegative. The first factor is simply the difference of the cell volume and the outgoing fluxed volumes. The second factor is the limited mass density at the position $\mathbf{r}_j^\star$. Let us discuss these two factors briefly.

The first factor is a restriction even in the case of a first-order scheme. The implications on the Courant numbers depend on the approximation one makes to the flux volumes. Take, for example, the case of the two-dimensional Cartesian mesh. Suppose one approximates the flux volumes as rectangular slabs adjacent to the cell faces with a volume equal to the fluxed volume through each face. In this case, one finds a stability condition such that the sum of the Courant numbers $\sigma_x = u\Delta t/\Delta x$ and $\sigma_y = v\Delta t/\Delta y$ must be less than one; a result which is well known [3–5].

Suppose one now takes into account the geometrical shapes and destinations of the fluxed volumes shown in Fig. 1. One then finds the restriction on Courant numbers is instead $\sigma_x < 1$, $\sigma_y < 1$, which has also been shown by previous investigators [3–5].

Now let us consider the second factor in Eq. (3.2.16), the limited mass density at $\mathbf{r}_j^\star$. Since we are using limited gradients to compute the density, the only requirement for nonnegativity is that $\mathbf{r}_j^\star$ be inside the cell. This will guarantee a nonnegative mass density. Whether $\mathbf{r}_j^\star$ is inside the cell or not will depend on parameters such as Courant numbers and the assumptions made concerning the shapes of the fluxed volumes. If one uses, for example, the slab approximation for the Cartesian mesh example, then one can show that the Courant numbers must satisfy $\sigma_x < (1-\sigma_y)^2$ and $\sigma_y < (1-\sigma_x)^2$ to assure nonnegativity. For $\sigma_x = \sigma_y = \sigma$ we have $\sigma < (3-\sqrt{5})/2 \approx 0.382$ to assure nonnegativity.

If, on the other hand, one uses a more realistic geometry with no overlapping volumes as shown in Fig. 1 then $\mathbf{r}_j^\star$ is simply $\langle \mathbf{r}_j \rangle_{re}$, which is always contained within the cell. In this case no additional Courant number limitations are imposed beyond those associated with the first factor on the right-hand side of Eq. (3.2.16).

Having set forth the conditions under which $0 \le Q \le 1$, the next task is to show that $\hat{T}_{in}$ and $\hat{T}_{re}$ are bounded by the local cell temperatures at time t^n.

3.3. *Inflow*

We treat the case of $\hat{T}_{in}$ first. Let us begin by defining the average temperature of the material in the ith inflow volume from neighbor cell m as

$$\tilde{T}_{i(m)} \equiv \frac{\langle \rho T \rangle_{i(m)}}{\langle \rho \rangle_{i(m)}}. \tag{3.3.1}$$

The subscript i denotes the ith inflow volume; the parenthetical subscript m has been added to denote the index of the donating neighbor cell. From Eq. (3.2.5) we can see that $\hat{T}_{in}$ is a weighted average of the inflow average temperatures, $\tilde{T}_{i(m)}$. (Note that the factor $\langle \rho \rangle_i / \{\sum_i \langle \rho \rangle_i \Delta V_i\}$ in Eq. (3.2.5) is the fraction of the inflowing mass from the ith inflowing fluxed volume. These factors are nonnegative and sum to one.) Thus $\hat{T}_{in}$ is bounded by the $\tilde{T}_{i(m)}$. Now if we show that the $\tilde{T}_{i(m)}$ are bounded by the jth cell and surrounding cell

temperatures, then we will have proved that $\hat{T}_{in}$ is bounded by the surrounding cell-center temperature data. From Eqs. (3.1.5) and (3.2.9) we may write the inflow mass from neighbor cell m as

$$\langle \rho \rangle_{i(m)} = \rho_m + (\nabla \rho)_m \cdot \langle \mathbf{r}_m \rangle_{i(m)}, \tag{3.3.2}$$

where $\langle \mathbf{r}_j \rangle_{i(m)}$ is the centroid of the fluxed volume, ΔV_i, from the donating cell m. The multidimensional linear expansion of $A = \rho T$—the analog of Eq. (2.3.1)—for each cell in the mesh is

$$\rho T = [\rho_j + \mathbf{r}_j \cdot (\nabla \rho)_j] T_j + \rho_j \mathbf{r}_j \cdot (\nabla T)_j. \tag{3.3.3}$$

From Eqs. (3.3.3) and (3.1.5) the fluxed energy takes the form

$$\langle \rho T \rangle = \langle \rho \rangle T_j + \rho_j (\nabla T)_j \cdot \langle \mathbf{r}_j \rangle. \tag{3.3.4a}$$

For the case at hand, the inflow energy from neighbor cell m is

$$\langle \rho T \rangle_{i(m)} = \langle \rho \rangle_{i(m)} T_m + \rho_m (\nabla T)_m \cdot \langle \mathbf{r}_m \rangle_{i(m)}. \tag{3.3.4b}$$

It is important to remember here that the mass density and temperature gradients in Eqs. (3.3.2)–(3.3.4b) are assumed to be limited. In particular, the extrema in each of the segments of the piecewise-nonlinear temperature field implied by the linear expansion (3.3.3),

$$T = T_j + \frac{\rho_j \mathbf{r}_j \cdot (\nabla T)_j}{\rho_j + \mathbf{r}_j \cdot (\nabla \rho)_j}, \tag{3.3.5}$$

should be bounded by surrounding mesh data. We note here that the Dukowicz–Kodis generalization of van Leer's limiter can be used to limit the temperature gradient, as well as the mass density gradient. This is done by using Eq. (3.3.5) with trial temperature gradients and limited mass density gradients to compute trial vertex temperatures. These vertex temperatures are then used in Eqs. (3.2.10b)–(3.2.10d) to compute a limiter coefficient, α_j. The limited temperature gradient is then simply the product of the limiter coefficient and the trial temperature gradient,

$$(\nabla T)_j \to \alpha_j (\nabla T)_j.$$

The temperature gradient limiter coefficient is generally different from the one used to limit the mass density gradient. Also, other gradient limiting procedures can be used so long as the extrema of the segments of the piecewise-nonlinear temperature field remain bounded by the surrounding mesh data.

It is worth pointing out here that the nonlinear temperature field given by Eq. (3.3.5) does not exhibit local extrema so we are assured that the cell vertex values give the extreme values for the temperature within each cell. Finally, since the temperature and mass densities used to construct the energy fluxes are bounded quantities, so then is the piecewise energy density field. Thus the new flux formulation will preserve the monotonicity characteristics of the van Leer advection scheme.

Using Eqs. (3.3.2), (3.3.4b) we can now compute the average temperature of the fluxed material:

$$\tilde{T}_{i(m)} \equiv \frac{\langle \rho T \rangle_{i(m)}}{\langle \rho \rangle_{i(m)}} = T_m + \frac{\rho_m (\nabla T)_m \cdot \langle \mathbf{r}_m \rangle_{i(m)}}{\rho_m + (\nabla \rho)_m \cdot \langle \mathbf{r}_m \rangle_{i(m)}}. \tag{3.3.6}$$

Comparing Eq. (3.3.6) with Eq. (3.3.5) shows that the average temperature of the fluxed material depends on the position of the fluxed volume centroid in an identical manner to the way that the temperature in the cell depends on position. If the temperature gradients are limited using the nonlinear temperature functionality of Eq. (3.3.5), we are assured that the average temperature of the fluxed material is bounded by the surrounding data.

Using the arguments put forward above, we can now see that the average inflow temperature, $\hat{T}_{in}$, will be a bounded quantity.

3.4. *Outflow*

We now turn our attention to the proof of the boundedness of $\hat{T}_{re}$, the temperature of the remaining material in the cell considering outflow only. We start with Eq. (3.2.4) and subtract the quantity $T_j \sum_o \langle \rho \rangle_o \Delta V_o$ from the first term in the numerator and add it to the second term:

$$\begin{aligned} \hat{T}_{re} &= \frac{T_j \left[\rho_j V_j - \sum_o \langle \rho \rangle_o \Delta V_o \right] - \sum_o [\langle \rho T \rangle_o - \langle \rho \rangle_o T_j] \Delta V_o}{\rho_j V_j - \sum_o \langle \rho \rangle_o \Delta V_o} \\ &= T_j + \frac{-\sum_o [\langle \rho T \rangle_o - \langle \rho \rangle_o T_j] \Delta V_o}{\rho_j V_j - \sum_o \langle \rho \rangle_o \Delta V_o}. \end{aligned} \tag{3.4.1}$$

Now if we use Eqs. (3.2.9) and (3.3.4a) we find

$$\langle \rho T \rangle_o - \langle \rho \rangle_o T_j = \rho_j (\nabla T)_j \cdot \langle \mathbf{r}_j \rangle_o. \tag{3.4.2}$$

Using Eq. (3.4.2) in Eq. (3.4.1) we obtain

$$\hat{T}_{re} = T_j + \rho_j (\nabla T)_j \cdot \frac{-\sum_o \langle \mathbf{r}_j \rangle_o \Delta V_o}{\rho_j V_j - \sum_o \langle \rho \rangle_o \Delta V_o}. \tag{3.4.3}$$

If we now use Eq. (3.3.2) to substitute for the fluxed mass, we find that

$$\hat{T}_{re} = T_j + \rho_j (\nabla T)_j \cdot \frac{-\sum_o \langle \mathbf{r}_j \rangle_o \Delta V_o}{\rho_j \left[V_j - \sum_o \Delta V_o \right] - (\nabla \rho)_j \cdot \sum_o \langle \mathbf{r}_j \rangle_o \Delta V_o}. \tag{3.4.4}$$

Finally, if we use definition (3.2.12) in Eq. (3.4.4) we obtain the simple relationship:

$$\hat{T}_{re} = T_j + \frac{\rho_j (\nabla T)_j \cdot \mathbf{r}_j^\star}{\rho_j + (\nabla \rho)_j \cdot \mathbf{r}_j^\star}. \tag{3.4.5}$$

Comparison of Eqs. (3.4.5) and (3.3.5) reveals that temperature of the remaining material in the cell should be bounded by the surrounding data as long as $\mathbf{r}_j^\star$ is within the jth cell and the temperature gradients are limited, so the extrema of the segments of the piecewise-nonlinear

cell temperature field remain bounded by surrounding mesh data. The restriction on $\mathbf{r}_j^\star$ is the same as put forward previously for the nonnegativity of m_{re} and, therefore, imposes the same restrictions on quantities such as Courant numbers to ensure monotonicity and compatibility.

To recap, the preceding analysis presents a method for obtaining multidimensional monotonic and compatible fluxes with the following restrictions:

First, the extrema of the segments of the piecewise-linear mass density and piecewise-nonlinear temperature fields at time t^n must be bounded by the surrounding mesh data. Second, the fluxed energies, $\langle \rho T \rangle$, must be computed using the expansion given by Eq. (3.3.4a). Third, the sum of the outflowing fluxed volumes from any cell in the mesh cannot exceed the total cell volume. Finally, the quantity $\mathbf{r}_j^\star$, defined by Eq. (3.2.12), must be contained within each respective cell.

At this point, one can further observe the behavior of the van Leer advection algorithm with the newly developed compatible flux formulation for compressible flow fields. The main observation is that the proof of compatibility and the compatible flux formulation presented in this section is fully general and includes the case of compressible flow fields. Compatibility will be maintained in any flow field, provided time steps are restricted so that the remaining mass—defined by Eq. (3.2.16)—remains nonnegative. Consider the limiting case in which a computational cell is completely emptied by a divergent flow field. In this case, the temperature of the cell will be driven to the temperature T_{re} given by Eq. (3.4.5). Because of the new compatible flux formulation, this temperature is guaranteed to be bounded by the surrounding temperature data and remains compatible. The behavior of the mass density is also interesting to examine for this case. The mass density for the emptying cell at time $n+1$ is given by

$$\rho_j^{n+1} = \frac{m_{re}}{V_j} = \left[\frac{V_j - \sum_o \Delta V_o}{V_j} \right] (\rho_j + (\nabla \rho)_j \cdot \mathbf{r}_j^\star) \to 0.$$

Because of the limiting of the mass density gradient and because of time step restrictions, the algorithm will never give unphysical negative mass densities. Thus, the advection scheme with the new compatible flux formulation is well suited to compressible flows.

4. EXAMPLE PROBLEMS

As an example problem, we consider the coupled system of equations

$$\frac{\partial}{\partial t} \begin{bmatrix} \rho_1 \\ \rho_2 \\ \rho_1 c_1 T_1 \\ \rho_2 c_2 T_2 \end{bmatrix} + \nabla \cdot \begin{bmatrix} \rho_1 \\ \rho_2 \\ \rho_1 c_1 T_1 \\ \rho_2 c_2 T_2 \end{bmatrix} \mathbf{u} = \begin{bmatrix} 0 \\ 0 \\ \rho_1 \rho_2 R(T_2 - T_1) \\ \rho_1 \rho_2 R(T_1 - T_2) \end{bmatrix}, \tag{4.1}$$

where R is a coupling parameter and c_1 and c_2 are specific heats. This system of equations describes a simple two-phase flow in which each phase is transported with the common constant velocity, $\mathbf{u}$, but with separate densities and temperatures. The subscripts denote the phases. We choose the two-phase system to provide an example in which mass densities are zero in parts of the domain but temperatures remained well-defined. The coupling terms on the right-hand side of equation system (4.1) ensure well-defined temperatures even in

the limit $\rho_k \to 0$, $k = 1$ *or* 2. This occurs because each term in the temperature equations is proportional to the phase mass density. In the test problems that follow, we will consider the tight coupling limit $R \to \infty$.

Since the equation system (4.1) has a nonzero right-hand side, a slight generalization of the method discussed above is required for solution. This involves the introduction of a time-split procedure. In the first step the solution is advanced using only the sources from the right-hand side of the equations. This step is called the Lagrangian step. In the second step, the solution is advanced from the Lagrangian data produced in the Lagrangian step using the procedures developed in this paper with no source terms. The second step is sometimes called the remapping step and includes any effects of compression and expansion from divergent velocity fields.

The following outlines the time-split procedure. Consider the generalized form of the transport equations in system (1.1),

$$\frac{\partial q}{\partial t} + \nabla \cdot q\mathbf{u} = f, \tag{4.2}$$

where q is a density. The quantity f represents source terms. The control volume description for this conservation equation is

$$\frac{d}{dt} \int_{V(t)} q \, dV + \int_{S(t)} q(\mathbf{u} - \mathbf{u}_s) \cdot \mathbf{n} \, dS = \int_{V(t)} f \, dS, \tag{4.3}$$

where the meaning of the symbols are the same as in Eq. (3.1.1). As in Section 3, we confine our attention to a stationary mesh control volume, V_j, with a zero mesh velocity ($\mathbf{u}_s = 0$). Letting qV denote $\int_V q \, dV$, Eq. (4.3) becomes

$$\frac{d(qV)_j}{dt} = -\int_{S_j} q\mathbf{u} \cdot \mathbf{n} \, dS + \int_{V_j} f \, dS. \tag{4.4}$$

In our time-split procedure we advance the cell averages first by considering the source terms only:

$$(qV)_j^L = (qV)_j^n + \Delta t \int_{V_j} f \, dS. \tag{4.5}$$

The superscript L denotes the Lagrangian data from the first or Lagrangian step. The solution is then obtained from the Lagrangian data considering the effect of the advection terms only,

$$q_j^{n+1} V_j = (qV)_j^{n+1} = (qV)_j^L - \Delta t \int_{S_j} q^* \mathbf{u} \cdot \mathbf{n} \, dS, \tag{4.6}$$

where q^* is a piecewise density field constructed using the methods described in this paper from cell-center data defined as $q_j^* = (qV)_j^L / V_j^n$. The q_j^* can be thought of as the average density of the Lagrangian state on the control volume V_j^n.

One can see that Eqs. (3.1.3) and (4.6) are essentially the same. The distinction between the two is that Eq. (4.6) operates on the Lagrangian data from the first step of the time-split method. Of course, in the absence of source terms, Eq. (4.6) is identical to (3.1.1).

In what follows we consider the advection of square-wave mass distributions in both one and two dimensions to illustrate the behavior of the new flux formulations. We choose mass densities of fields one and two to be 1 and 0.001, respectively. This gives the system the character of a liquid–gas multiphase flow. Furthermore, we choose the specific heats to be 1 and 1000 so the product of material density and specific heats are equal; this gives the temperatures symmetry with respect to energy.

We will compare the following cases:

(1) a first-order method;

(2) a standard application of van Leer's second-order method using a linear expansion for the energy density, that is Eq. (2.1.5) with $q = \rho T$, and using the linear limited difference operator given by Eq. (2.1.6). This is the case corresponding to the discussion in Section 2.2;

(3) a second-order method using the expanded flux form for energy density given by Eqs. (2.3.6a)–(2.3.6b) but using the linear limited difference operator given by Eq. (2.1.6) for both the mass density and temperature; and

(4) a *compatible* second-order method using the expanded flux form for energy density given by Eqs. (2.3.6a), (2.3.6b) using the linear limited difference operator for mass density and the nonlinear limited difference operator given by Eq. (2.3.4a)–(2.3.4b) for the temperature.

4.1. *Advection of a One-Dimensional Square Wave*

We first consider the solution of equation system (4.1) on a one-dimensional domain 100 units long. We discretize the domain into 100 units so all $\Delta x_j = 1$. The x component of velocity is taken as a positive constant, $u = 1$. The initial mass densities and temperatures are distributed at time $t = 0$ as shown in Table I.

The boundary conditions on mass density and temperature are Neumann. The exact solution of the equation system for these boundary and initial conditions is simply a rigid body motion of the density and temperature fields to the right with the velocity $u = 1$.

We performed calculations for Courant numbers of 0.10 and 0.999. The smaller Courant number was chosen to examine the numerical diffusion characteristics in the three cases. The larger Courant number was chosen to give a high weighting to the face value contribution for the "remaining" temperature. (See Eqs. (2.3.11a), (2.3.11b).

The results from our computations at $t = 50$ time units are shown in Figs. 2a through 5c.

As one can see from the figures, both the standard van Leer case and the expanded flux formulation with linear temperature field gradient limiting produce noncompatible temperatures. Only the expanded flux formulation with nonlinear temperature field gradient limiting produces compatible temperatures with second-order accuracy. Note also that the nonlinear gradient limiting does not appear to introduce diffusive behavior beyond that seen in the other second-order cases.

TABLE I

Field	$x < 10$	$10 \le x \le 30$	$30 < x$
ρ_1	1	0	1
ρ_2	0	10^{-3}	0
T_1	0	1	0
T_2	0	1	0

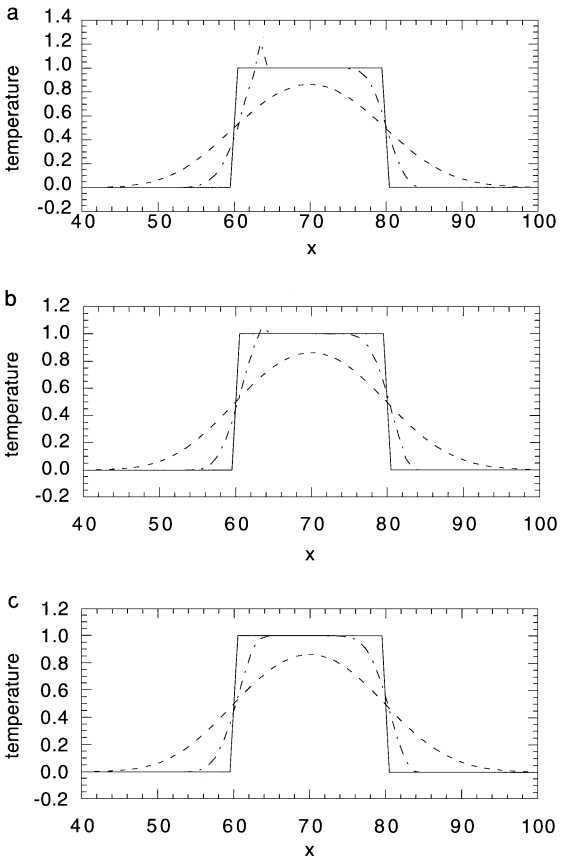

FIG. 2. Field 1 temperatures, $\sigma = 0.1$ (———, analytic; - - - -, 1st order; —·—·—·, 2nd-order): (a) standard van Leer, (b) expanded flux, linear temperature field, (c) expanded flux, nonlinear temperature field.

4.2. *Advection of a Notched Two-Dimensional Box*

We will now demonstrate the multidimensional capabilities of the new flux formulation by computing the advection of a notched two-dimensional box. We use a notched box to provide a more intricate configuration for the demonstration. We will use an accurate, nonoverlapping geometric description of the flux volumes so that the Courant numbers σ_x and σ_y can both approach one. We show that the box is advected with compatible temperatures for case 4 but not for case 3. We first discuss the problem specification and then the flux volume computation, followed by the results of the computation.

Consider the two-phase flow system described in the previous section in a two-dimensional square domain with dimensions 100 units by 100 units. Let both phases have a uniform velocity field with x and y components equal to one so that flow is along the diagonal of the domain. The mass densities and temperatures are distributed at time $t = 0$ as shown in Fig. 6.

The boundary conditions on density, velocity, and temperature are Neumann.

As in the one-dimensional case, the analytical solution to the governing differential equations is such that the box simply translates as a rigid body along the diagonal of the domain. Since there is no heat diffusion, the temperature fields also translate with the same rigid body motion.

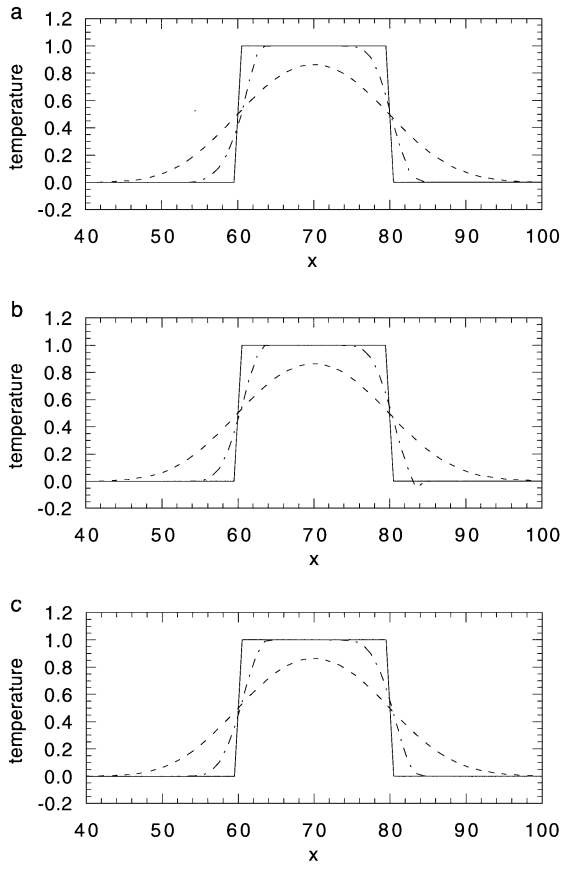

FIG. 3. Field 2 temperatures, $\sigma = 0.1$ (———, analytic; - - - -, 1st order; —·—·—·—, 2nd-order): (a) standard van Leer, (b) expanded flux, linear temperature field, (c) expanded flux, nonlinear temperature field.

As in the one-dimensional case, the state variables were advanced using the Lagrangian form of the equations. The Lagrangian update is then advected solving equation system (4.1) with zero right-hand side. The advection step was unsplit with regard to mesh direction and consisted of visiting each cell face, computing the required mass and energy fluxes in the manner described above, and then moving these quantities from the donating cell to the appropriate accepting adjacent and corner cells as depicted in Fig. 1. The fluxes were computed using the Dukowicz–Kodis [8] gradient limiting procedure outlined above.

The flux volumes and centroids were computed from the physical picture presented in Fig. 1 as follows. Introduce a local ξ, η coordinate system, as shown in Fig. 7 so that $\xi = \eta = 0$ at the bottom-left corner of the cell and $\xi = \eta = 1$ at the top-right corner.

Consider the case of the flux volumes associated with the right face in Fig. 1. From the Courant numbers we locate the coordinates ℓ_1 and ℓ_2 as shown in Fig. 7 as $\ell_1 = 1 - \sigma_x$ and $\ell_2 = 1 - \sigma_y$. In ξ, η space, the flux volume through the face and the volumes of the triangular and the rectangular sections are

$$\Delta v_o = 1 - \ell_1, \quad \Delta v_{tri} = \frac{1}{2}(1 - \ell_1)(1 - \ell_2), \quad \Delta v_{rect} = \ell_2(1 - \ell_1).$$

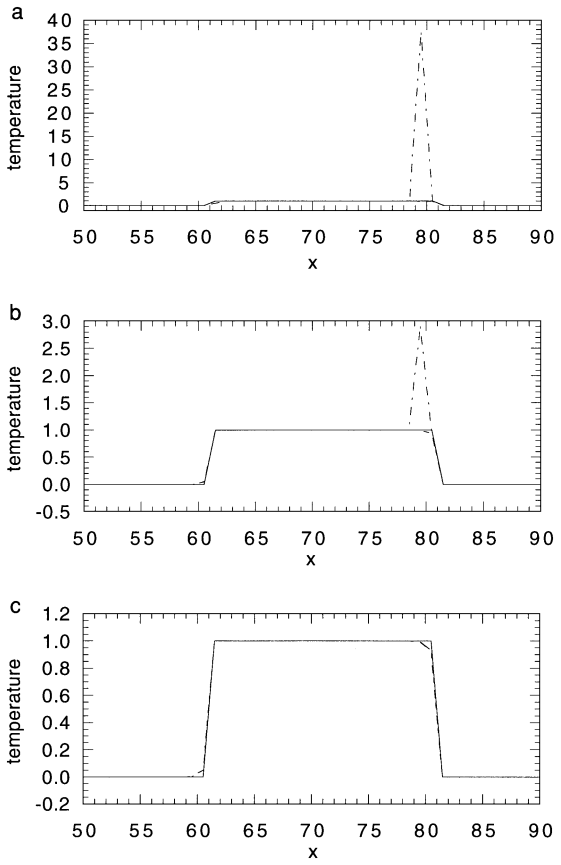

FIG. 4. Field 1 temperatures, $\sigma = 0.999$ (———, analytic; - - - -, 1st order; —·—·—·, 2nd-order): (a) standard van Leer, (b) expanded flux, linear temperature field, (c) expanded flux, nonlinear temperature field.

The centroids of the triangular and rectangular sections in ξ, η coordinates are

$$\xi^c_{tri} = \frac{2}{3} + \frac{1}{3}\ell_1, \quad \eta^c_{tri} = \frac{1}{3} + \frac{2}{3}\ell_2$$

and

$$\xi^c_{rect} = \frac{1}{2} + \frac{1}{2}\ell_1, \quad \eta^c_{rect} = \frac{1}{2} + \frac{1}{2}\ell_2.$$

The centroids in physical space can be found with the simple mapping

$$r_x = \frac{\Delta x}{2}(2\xi - 1), \quad r_y = \frac{\Delta y}{2}(2\eta - 1).$$

With the foregoing equations, the fluxed mass and energy from the triangular and rectangular portions of the fluxed volumes were computed. The portion of the fluxed quantities associated with the triangle were added to the cell sharing only a corner. The rectangular portion was added to the adjacent cell. Note that the other triangular portion, Section 7 in Fig. 1, was not fluxed when treating the right face of cell j. This piece is treated with the upper face of the cell below cell j. The above scheme can be shown to be equivalent to van Leer's multidimensional scheme [2].

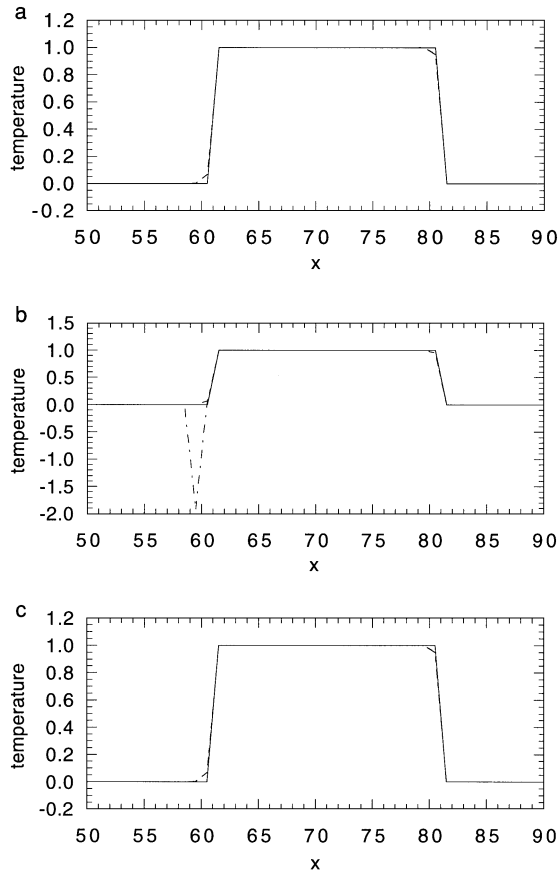

FIG. 5. Field 2 temperatures, $\sigma = 0.999$ (———, analytic; - - - -, 1st order; —·—·—·, 2nd-order): (a) standard van Leer, (b) expanded flux, linear temperature field, (c) expanded flux, nonlinear temperature field.

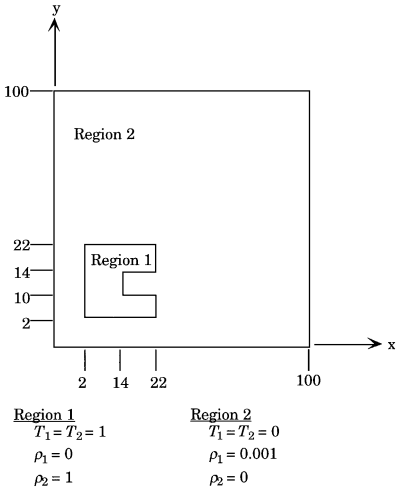

FIG. 6. Initial conditions.

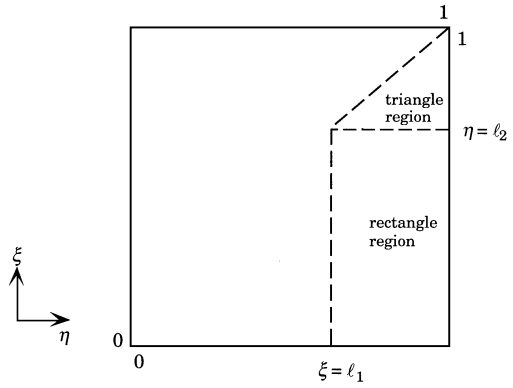

FIG. 7. Local coordinates.

Using these methods, two second-order calculations were performed corresponding to cases 3 and 4 to illustrate the performance of the nonlinear temperature gradient limiting. (The standard van Leer case gave noncompatible solutions similar in character to that seen in the one-dimensional example and are not shown here.) Both calculations were performed for Courant numbers of $\sigma_x = \sigma_y = 0.999$. These high values were chosen to accentuate the noncompatibility of the linear gradient limiting scheme, case 3. Computations were also performed for Courant numbers of $\sigma_x = \sigma_y = 0.1$ for cases 3 and 4. We do not show these results here since the noncompatibility in case 3 was difficult to see in the multidimensional perspective plots used to display results.

The results of the advection calculations are shown in Figs. 8a–d. In all figures, the initial and final results are plotted together. The initial state is shown on the left side of the figures and the final state at a time of 65 time units is shown on the right.

The temperature fields from the linear gradient limiting calculations are shown in Figs. 8a–b. Significant overshoot and undershoot are seen. The temperature fields from the calculation with nonlinear gradient limiting are shown in Figs. 8c–d. Here we see no overshoot nor undershoot, as predicted by the analysis.

5. CONCLUSIONS

We have formulated new fluxes for the second-order van Leer advection operator. These fluxes preserve monotonicity of computed density fields *and* ensure compatibility of transport quantities such as velocity, temperature, energy, and species concentration while retaining second-order accuracy in the usual sense. The key to the new method is to expand the densities as a linear function within each cell. For the flux of any quantity, ρT, which is the product of density and the transported quantity, the gradient is then expanded using the product rule. The ρT flux computed from the expansion can then be written as the product of a second-order mass flux with the cell-center temperature plus a term proportional to ∇T. Monotonicity of ρT and compatibility of T are then ensured if the gradient of T is limited using the nonlinear spatial distribution for T implied by the linear expansions for ρ and ρT. This method is extendable to higher-order schemes with nonlinear density distributions. The method as derived for the multidimensional case is fully general, and therefore applicable,

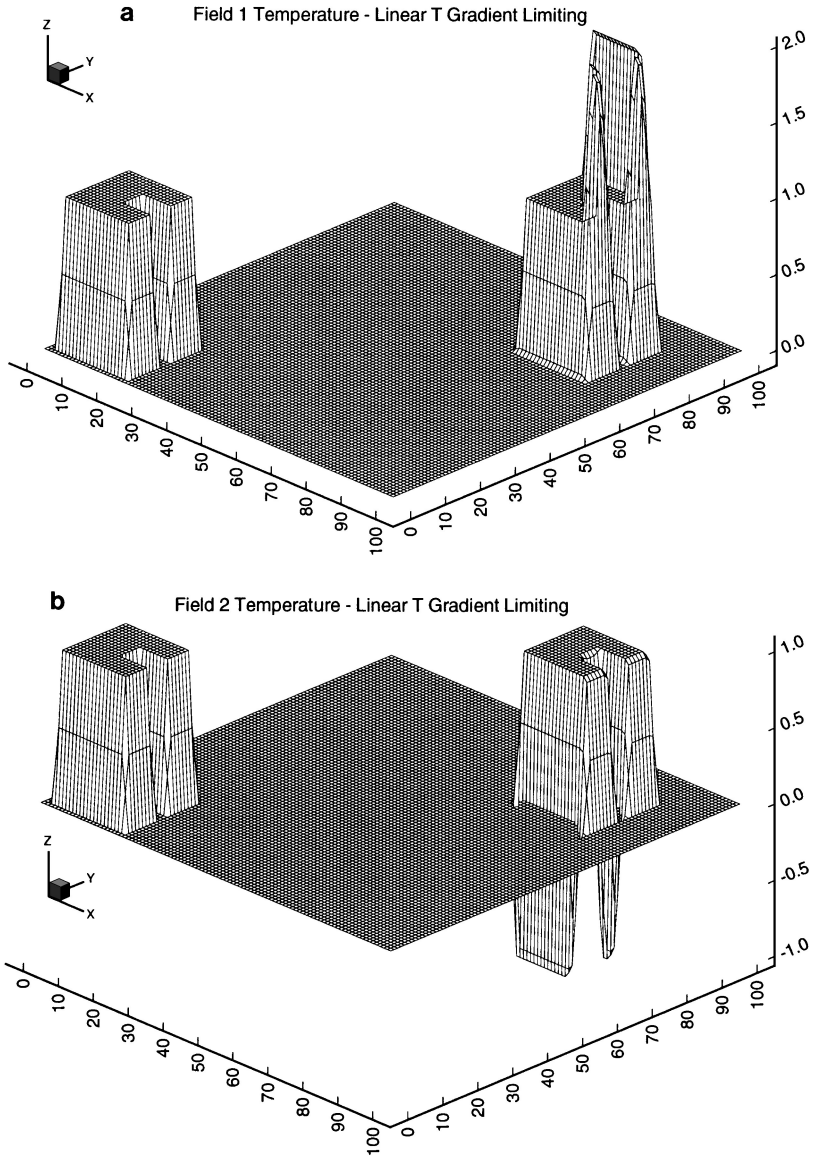

FIG. 8. (a) Field 1 temperature with linear gradient limiting; (b) Field 2 temperature with linear gradient limiting; (c) Field 1 temperature with non-linear gradient limiting; (d) Field 2 temperature with nonlinear gradient limiting.

to the cases with nonuniform velocity fields and arbitrary control volume geometry. Also, this method should permit the use of a variety of gradient limiting procedures, in addition to that of Dukowicz and Kodis, [8], used in this paper.

6. FUTURE WORK

One can imagine several possible extensions of this work. First, the method should apply directly to compressible flows. We did not include a compressible flow example in this

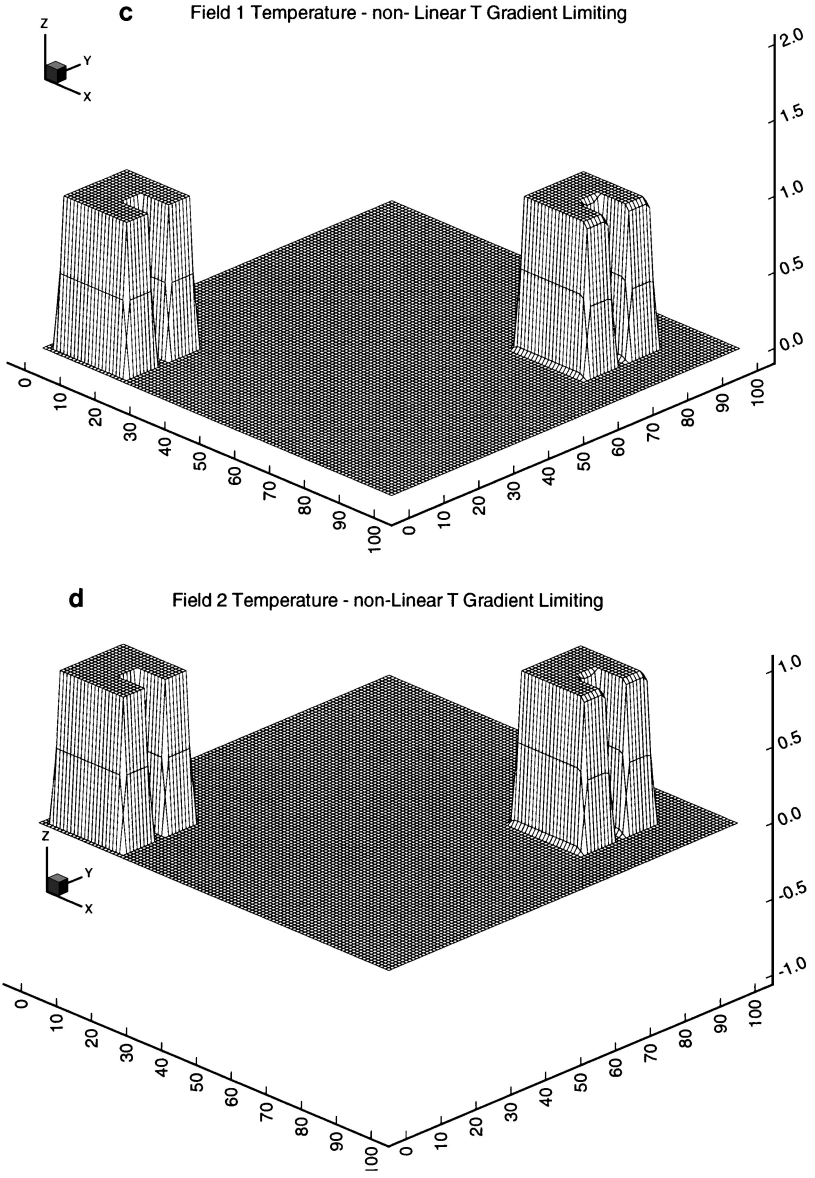

FIG. 8—*Continued*

paper as it is already lengthy. A demonstration of the method for a suitable compressible flow would be an obvious next step. In addition, the method outlined here should work on unstructured meshes. An example calculation on a suitable unstructured mesh would be another interesting followup item.

Another obvious extension of this work is to examine compatibility in cases for which the conserved quantity is a more complicated function of mass-specific transport quantities. A common example is the total energy given by the sum of internal and kinetic energy,

$$\rho E = \rho\left(T + \frac{1}{2}\mathbf{u}\cdot\mathbf{u}\right).$$

For this case, the flux of ρE can be computed from the expanded expression

$$\rho E = \left[T_j + \frac{1}{2}\mathbf{u}_j \cdot \mathbf{u}_j\right][\rho_j + (\nabla\rho)_j \cdot \mathbf{r}_j] + \rho_j[(\nabla T)_j + \mathbf{u}_j \cdot (\nabla\mathbf{u})_j] \cdot \mathbf{r}_j.$$

The temperature and velocity gradients should be limited so that the piecewise-nonlinear velocity and temperature fields given by

$$\mathbf{u} = \mathbf{u}_j + \frac{\rho_j(\nabla\mathbf{u})_j \cdot \mathbf{r}_j}{[\rho_j + (\nabla\rho)_j \cdot \mathbf{r}_j]}$$

and

$$T = T_j + \frac{\rho_j(\nabla T)_j \cdot \mathbf{r}_j}{[\rho_j + (\nabla\rho)_j \cdot \mathbf{r}_j]} - \frac{1}{2}\frac{\rho_j(\nabla\mathbf{u})_j \cdot \mathbf{r}_j}{[\rho_j + (\nabla\rho)_j \cdot \mathbf{r}_j]} \cdot \frac{\rho_j(\nabla\mathbf{u})_j \cdot \mathbf{r}_j}{[\rho_j + (\nabla\rho)_j \cdot \mathbf{r}_j]}$$

remain bounded by surrounding mesh data. It is then straightforward to explore the implications of such a strategy on the compatibility of the resulting advection scheme. Other future work might explore the implications of the techniques developed in this paper on implicit schemes and on higher-order schemes.

ACKNOWLEDGMENTS

We gratefully acknowledge support for this work from the U.S. Department of Energy. We also thank J. K. Dukowicz, P. J. O'Rourke, N. L. Johnson, R. M. Rauenzahn, and D. B. Kothe for their encouragement and helpful suggestions.

REFERENCES

1. C. Schär and P. K. Smolarkiewicz, A synchronous and iterative flux-correction formalism for coupled transport, *J. Comput. Phys.* **128**, 101 (1996).
2. J. Thuburn, Multidimensional flux-limited advection schemes, *J. Comput. Phys.* **123**, 74 (1996).
3. B. van Leer, Multidimensional explicit difference schemes for hyperbolic conservation laws, in *Computing Methods in Applied Sciences and Engineering VI*, edited by R. Growinski and J. L. Lions (Elsevier, Amsterdam, 1984).
4. P. Collela, Multidimensional upwind methods for hyperbolic conservation laws, *J. Comput. Phys.* **87**, 171 (1990).
5. J. Saltzman, An unsplit upwind method for 3D hyperbolic conservation laws, *J. Comput. Phys.* **115**, 153 (1994).
6. R. J. Leveque, High-resolution conservative algorithms for advection in incompressible flow, *SIAM J. Numer. Anal.* **33**, 627 (1996).
7. B. van Leer, Towards the ultimate conservative difference scheme. IV. A new approach to numerical convection, *J. Comput. Phys.* **23**, 276 (1977).
8. J. K. Dukowicz and J. W. Kodis, Accurate conservative remapping, *SIAM J. Sci. Stat. Comput.* **31**, 305 (1987).
9. B. van Leer, Towards the ultimate conservative difference scheme. V. A second-order sequel to Godunov's method, *J. Comput. Phys.* **31**, 101 (1979).
10. P. A. Thompson, *Compressible Fluid Dynamics*, McGraw–Hill, New York, 1972.